# Time evolution analysis of the electron distribution in Thomson/Compton back-scattering

V. Petrillo, A. Bacci, C. Curatolo, C. Maroli, L. Serafini et al.

Citation: J. Appl. Phys. **114**, 043104 (2013); doi: 10.1063/1.4816683
View online: http://dx.doi.org/10.1063/1.4816683
View Table of Contents: http://jap.aip.org/resource/1/JAPIAU/v114/i4
Published by the AIP Publishing LLC.

JOURNAL OF APPLIED PHYSICS **114**, 043104 (2013)

# Time evolution analysis of the electron distribution in Thomson/Compton back-scattering

V. Petrillo, A. Bacci, C. Curatolo, C. Maroli, L. Serafini, and A. R. Rossi[a)]
*INFN-Universitá degli Studi Milano, Via Celoria, 16 20133 Milano, Italy*

(Received 8 May 2013; accepted 11 July 2013; published online 24 July 2013)

We present the time evolution of the energy distribution of a relativistic electron beam after the Compton back-scattering with a counter-propagating laser field, performed in the framework of the Quantum Electrodynamics, by means of the code CAIN. As the correct angular distribution of the spontaneous emission is accounted, the main effect is the formation of few stripes, followed by the diffusion of the more energetic particles toward lower values in the longitudinal phase space. The Chapman-Kolmogorov master equation gives results in striking agreement with the numerical ones. An experiment on the Thomson source at SPARC-LAB is proposed. © *2013 AIP Publishing LLC*. [http://dx.doi.org/10.1063/1.4816683]

## I. INTRODUCTION

The availability of radiation characterized by short wavelength, high brilliance, large transverse coherence, monochromatic spectrum, and wide tunability opens the way for a new era in physics, chemistry, and bio-medicine since these pulses permit to detect objects and to control processes at the atomic length scale. Many applications in different fields of physics, as for instance advanced imaging techniques, crystallography, exploration of matter, plasmas, high energy systems, and nuclear photonics, require quasi-monochromatic X and $\gamma$ radiations with large spectral intensity. Besides synchrotrons,[1] free-electron lasers,[2–5] and high-order harmonic generation driven by lasers in gases,[6] Thomson and Compton sources are among the most performing devices for producing radiation with the aforementioned qualities.

Thomson and Compton sources[7–10] are based on the back-scattering between the light pulse of a large intensity laser and a high brightness, high energy electron beam produced by a linac.

During the interaction, the exchange of momentum between the electrons and the laser photons takes place, causing the emission of Doppler up-shifted X/$\gamma$ rays and, as a consequence, the deformation of the electron phase space structure. The time evolution of the electron energy distribution during and after the scattering process could be an important characteristic from both fundamental and diagnostic points of view, because it encodes several detailed informations about the nature and the feature of the collision. Furthermore, the possibility of assembling cascaded sources, driven by the same electron beam at different energy points, depends upon the degree of deterioration of the electron phase space after the scattering. In addition, there is also the possibility that, during the interaction, a cooling of the electron beam takes place.[11,12]

Despite these potential important perspectives, no systematic experimental measurements of the electron distribution have been so far carried on in Thomson and Compton sources.

From a theoretical point of view, the time evolution of the longitudinal phase space of the electrons in the Compton process has been considered in the old literature as an example of random walk,[13] where each step corresponds to the loss of an energy (or longitudinal momentum) quantum in the scattering event. The phenomenon is considered to belong to the Poisson's process ensemble and studied in Ref. 14 in the para-axial approximation, considering only the radiation emitted on axis. However, due to the three-dimensional nature of the Thomson/Compton scattering, with the well-known energy-angle correlation in the emitted photon phase space, a simple Poisson's equation is not suitable to describe the phenomenon. The most accredited model for the time evolution of the Compton electron energy distribution, in the framework of the quantum statistics, is the master equation derived from the Chapman-Kolmogorov equation,[15] containing an average on the photon energy. In the limit of numerous steps, corresponding to long times and/or emitted photons of limited energy, the master equation can be simplified in a diffusion equation,[16,17] which is evidence of classical statistical behavior. Within another philosophy, the electron distribution after the scattering can be studied by means of Monte Carlo codes based on the Klein-Nishina cross section,[10,21] such as CAIN,[19,20] which gives the photon and electron phase spaces under the effect of a realistic laser. Direct calculations of the electron energy,[18] performed with CAIN, show the time evolution of the electron distribution from the initial condition. At short times, the energy distribution develops a sequence of neat stripes, connected to the fact that the adopted model considers the scattering between an electron and a photon as a two point-particle collision. These structures have been never observed or foreseen before in Thomson/Compton sources and are connected to the point-like nature of the scattering. Later on, as the electrons undergo more collisions, a regime of continuous diffusion of the more energetic particles toward lower values of energy establishes.

[a)]Electronic address: petrillo@mi.infn.it

 

In this paper, we demonstrate that the master equation deduced from the Chapman-Kolmogorov model for Markov processes, with a suitable expression of the photon distribution, describes the details of the electron distribution during the Compton scattering process. We compare its solution with the simulation performed with CAIN showing a striking agreement. We will show that the master equation foresees the formation of stripes in energy that are signature of the point-like nature of the collision and that gradually evolve in a continuous structure. Then, we will present the realistic study of an experimental proof of this process at the Thomson source at SPARC-LAB. Conclusions and comments will end our paper.

## II. THE MODEL EQUATION

The evolution equation which rules the probability of making a number $m$ of transitions in a Poisson's phenomenon is

$$\frac{\partial P_m(t)}{\partial t} = a(P_{m-1}(t) - P_m(t)), \tag{1}$$

where $a$ is the collision rate. The solutions of (1) are the well-known Poisson's functions

$$P_m(at) = \frac{(at)^m e^{-at}}{m!}. \tag{2}$$

An equation that has been proposed[14,22] for modeling the energy distribution during the Compton process, assuming the momentum to be exchanged in fixed quanta $\beta$, is

$$\frac{\partial N(p,t)}{\partial t} = \alpha(N(p+\beta,t) - N(p,t)), \tag{3}$$

where $\alpha$, independent of time, is the rate of photon production.

Equation (3) can be solved by applying the Fourier transform with respect to $p$, and, by using the Anger-Jakobi expansion and the Bessel function properties, one can relate the momentum distribution at time $t$ to the initial condition

$$N(p,t) = \sum_{l=0,\infty} G_l(\alpha t) N(p + l\beta, t = 0), \tag{4}$$

where the functions

$$G_l(\alpha t) = e^{-\alpha t} \sum_{m=-\infty,\infty} I_{l-m}(\alpha t) J_m(\alpha t), \tag{5}$$

where $J_m$ and $I_m$ are Bessel and modified Bessel functions, which can be demonstrated to be equal to the Poisson's functions $P_l(\alpha t)$ defined in (2).

The use of Eq. (3) and the prevision of a neat momentum grouping that persists at long times[14,22] have been the object of discussion.[17,18,23,24] The criticisms to Refs. 14 and 22 were based on the fact that, in the Thomson/Compton scattering, the quantum $\beta$ does not have a fixed value, being distributed over a range between two values $\beta_{min}$ and $\beta_{max}$, determined by the momentum-angle correlation typical of the process.

The photon and the related emitted energy angle-integrated distribution functions, derived from the Klein-Nishina cross section, as a function of the momentum are shown in Fig. 1. The probability density of the photon emission at momentum $\pi$ during the scattering can be modeled as[25]

$$W(\pi, \pi_{min}) = \frac{3}{\Delta\pi}\left[\left(\frac{\pi - \pi_{min}}{\Delta\pi}\right)^2 - \frac{\pi - \pi_{min}}{\Delta\pi} + \frac{1}{2}\right] \times H(\pi_{max} - \pi) H(\pi - \pi_{min}), \tag{6}$$

where $\Delta\pi = \pi_{max} - \pi_{min}$, $H(x)$ are step-like Heaviside functions, and

$$\pi_{min} = \hbar\omega_L/c,$$

$$\pi_{max} = \frac{(1+\beta_e)\hbar\omega_L/c}{1 - \beta_e + 2\hbar\omega_L/(\gamma_e m_0 c^2)}$$

are, respectively, the momenta of the photons emitted forward and backward on axis, with $\beta_e = v_e/c$ the normalized velocity of the electron, $m_0$ the rest mass, $\gamma_e$ the Lorentz factor, and $\hbar\omega_L/c$ the laser photon momentum quantum.

The generalization of Eq. (3) to the case of a photon momentum distribution is derived in Refs. 15 and 26 from the Chapman-Kolmogorov equation for Markov phenomena and leads to the following expression:

$$\frac{\partial P(p,t)}{\partial t} = \alpha\left(\int dp^* W(p,p^*) P(p^*,t) - P(p,t)\right), \tag{7}$$

where $P$ is the probability of an electron being in a state with momentum $p$ at a time $t$ and $W$ is the transition probability per unit time from $p^*$ to $p$, which depends upon the physics of the phenomenon.

In the case of the Thomson/Compton scattering, $W$ can be approximated by Eq. (6), where $\pi = p$ and

$$\pi_{min} = p^*,$$

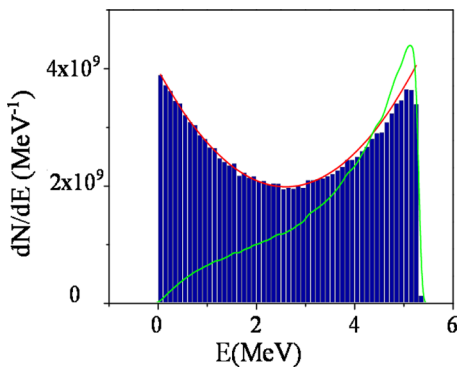


FIG. 1. Photon distribution $dN/dE(\text{MeV}^{-1})$ vs energy $E$ in MeV. On the left axis: navy columns: distribution of the emitted photons. On the right axis: green line: energy distribution of the radiation in arbitrary units. Red line: approximate expression of the photon distribution.

$$\pi_{max} = p^* - \frac{(1+\beta_e)\hbar\omega_L/c}{1-\beta_e+2\hbar\omega_L/(m_0\gamma_e c^2)}.$$

If the momentum of the laser photon can be considered negligible and the electron velocity is close to $c$ (i.e., $\gamma_e \gg 1$), thus the quantity $(1+\beta_e)/(1-\beta_e)$ is about $4\gamma_e^2$, the transition probability per unit time can be further simplified in

$$W(p,p^*) = \frac{3}{\left(4\frac{\hbar\omega_L}{c}\frac{p*^2}{m_0^2c^2}\right)}\left[\left(\frac{p^*-p}{4\frac{\hbar\omega_L}{c}\frac{p*^2}{m_0^2c^2}}\right)^2 - \frac{p^*-p}{4\frac{\hbar\omega_L}{c}\frac{p*^2}{m_0^2c^2}} + \frac{1}{2}\right] \times H\left(p^*-p-\frac{\hbar\omega_L}{c}\right) \times H\left(p-p^*+4\frac{\hbar\omega_L}{c}\frac{p*^2}{m_0^2c^2}\right). \quad (8)$$

Assuming that the solution of Eq. (7) is a linear combination of Poisson's functions

$$P(p,p_0,t) = \sum c_n(p,p_0)P_n, \quad (9)$$

choosing

$$c_0(p,p_0) = \delta(p-p_0),$$

the coefficients $c_n(p,p_0)$ satisfy the recurrence relation

$$c_{n+1}(p,p_0) = \int dp^* W(p,p^*)c_n(p^*,p_0). \quad (10)$$

The generic term

$$c_m(p,p_0) = \int dp_{m-1}..dp_n..dp_1 W(p,p_{m-1}) \times W(p_{n+1},p_n)..W(p_2,p_1)W(p_1,p_0) \quad (11)$$

is the probability per unit time of making the transition from $p_0$ to $p$ in a number $m$ of collisions, integrated over all the possible paths. The whole probability of reaching $p$ starting from $p_0$ is then the sum over all the number of steps compatible with the jump. The time evolution of the electron distribution $N(p,t)$ is obtained by a convolution of $P(p,p_0,t)$ with the initial condition $N(p_0,t=0)$.

Equation (7) has been solved numerically by means of a standard finite difference method or by means of Eqs. (9)–(11) and the results compared to the data provided by the Monte Carlo code CAIN,[19,20] a well-known code based on the Klein-Nishina cross section and widely validated in the case of Compton scattering by comparisons with experimental data[10] and analytical models.[10,21]

Figure 2 presents the results of this comparison for three different time values, showing a striking agreement. The energy of the electrons changes during the radiation emission due to the whole photon spectrum described by the function W. In the early stage of the emission (panels (a), (b)), trace of the quantum nature of the interaction is revealed by the

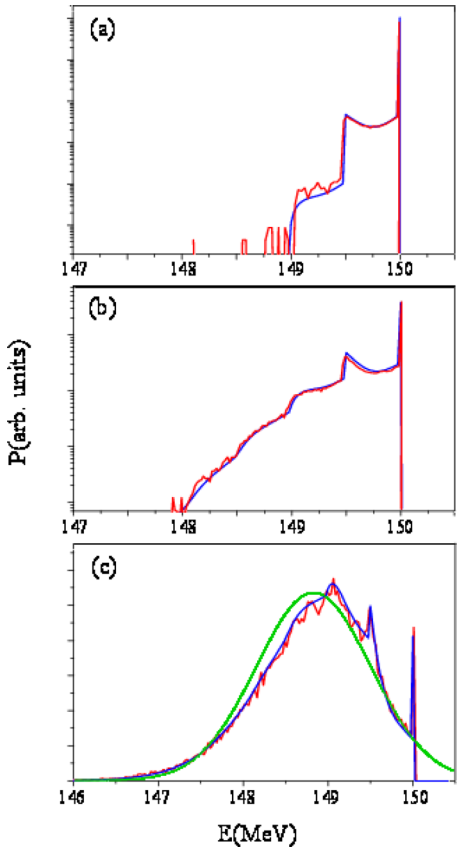


FIG. 2. Electron distribution function (in arbitrary units) vs energy (MeV) at different times (a) $t = 0.083$ ps, (b) $t = 1.66$ ps, (c) $t = 6.66$ ps and initial electron energy $E(t=0) = 150$ MeV. (a) and (b) Logarithmic scale, (c) linear scale. Red curves obtained by CAIN, blue curves from the integration of Eq. (7), green curve solution of Eq. (12).

gradual population of a number of stripes with energy lower than the initial one that rapidly merge in a diffusion structure (panel (c)). Most of the electrons do not undergo collisions and remain in their initial state at 150 MeV, while the peaks at 149.5 MeV and 149 MeV are due to electrons that have participated to one or two collisions. The stripe regime is due to the fact that the scattering is considered as the collision between two point-like particles, and the evolution of the phase space resembles a process of random walk.[13,18]

The diffusion regime can be obtained by developing $P$ for small $\Delta = p - p^*$ under the sign of integral in (7). The diffusion equation

$$\frac{\partial P(p,t)}{\partial t} = \frac{\partial(aP(p,t))}{\partial p} + \frac{1}{2}\frac{\partial^2(bP(p,t))}{\partial p^2}, \quad (12)$$

with $a = \int d\Delta \Delta W(p,\Delta)$ and $b = \int d\Delta \Delta^2 W(p,\Delta)$ (Ref. 26), has been solved in the limit of constant $a$ and $b$, evaluated at the initial point $p = p_0$, and the result superimposed to the others in Fig. 2, panel (c). The comparison between the effective result by CAIN and the solution of (12) shows that the classical regime is not yet completely achieved.

## III. ANALYSIS OF A POSSIBLE EXPERIMENT

In this paragraph, we present the analysis of an experiment aimed at exploring the point-like nature of the collision

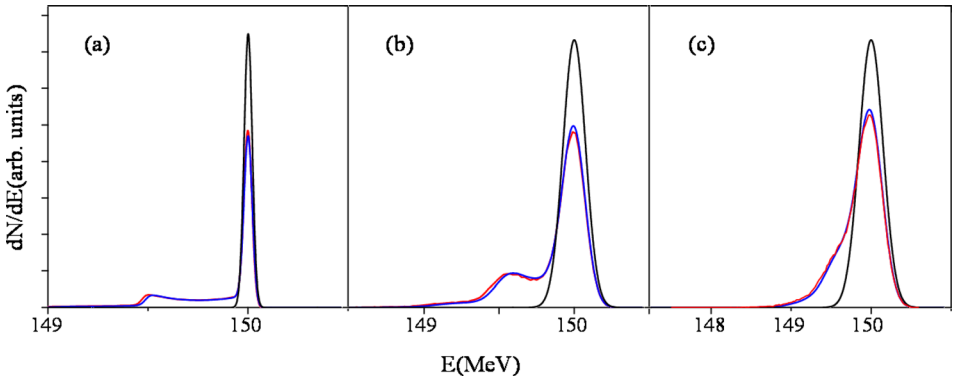


FIG. 3. Comparison between the data obtained by integrating Eq. (7) by means of Eqs. (9)–(11) using 6 terms (blue curve) and the CAIN results (red curve) with Gaussian initial condition (black curve) with increasing energy spread: (a) $\Delta E/E = 10^{-4}$, (b) $\Delta E/E = 5 \times 10^{-4}$, (c) $\Delta E/E = 10^{-3}$. Other data: $\Delta t_L = 2.4$ ps with $E_L = 0.75$ J.

TABLE I. Electron beam and laser pulse main characteristics.

| Quantity | Value |
|---|---|
| Charge (pC) | 250 |
| Energy (MeV) | 150 |
| Energy spread (MeV) | $10^{-4} - 10^{-3}$ |
| emittance (mm mrad) | 1–2 |
| Twiss $\beta$ parameter (mm) | 0.4 |
| Laser wavelength (nm) | 800 |
| Laser energy $E_L$(J) | 0.25–5 |
| Laser rms time duration $\Delta t_L$ (ps) | 0.8–16 |
| Laser Rayleigh length $R_L$ (mm) | 0.5 |
| Maximum photon energy (MeV) | 0.5 |
| Quantum red shift (keV) | 2 |

and the transition between a quantum statistical behavior associated to the presence of the stripe regime and the classical one, where the electron distribution tends to become a Gaussian function.

The results shown in Sec. II have been obtained in an ideal context with an electron initial distribution described by delta-like functions interacting with a laser without diffraction.

The presence of energy spread and emittance in the initial electron distribution, as well as a less simplified laser model, must be taken into account in the study of a possible experiment. The energy spread effect can be analyzed by solving Eq. (7) with a given initial condition. Fig. 3 shows the results obtained by imposing a Gaussian initial condition with increasing rms width.

Then we have studied the effects of the beam emittance and laser pulse diffraction by means of the code CAIN. The realistic example is the Thomson source PlasmonX[27,28] at SPARC-LAB,[4] operated at 150 MeV. The electron beam, whose main parameters are summarized in Table I, collides with the Ti:Sapphire Laser FLAME,[29] with wavelength $\lambda_L = 2\pi c/\omega_L = 800$ nm. The laser energy $E_L$ can reach 5 J and the pulse can be compressed up to 100 fs. In the proposed examples, the laser energy varies from 0.25 J to 5 J at fixed energy density value, with a laser rms time duration ranging from 0.8 ps to 16 ps. A critical issue for the detection of the stripe regime is the value of the electron energy spread $\Delta E/E$. Fig. 4 shows the effect of $\Delta E/E$ for the interaction with the laser pulse of variable length. With $\Delta E/E = 10^{-4}$, the first two stripes are clearly manifest, even if the second peak has disappeared. Increasing the initial energy spread of the beam, the stripes become less evident. For $\Delta E/E \approx 10^{-3}$, they cannot be anymore distinguished and the distribution appears continuous. This effect can be appreciated in the inner boxes of Fig. 4, where the distribution is displayed in the x-y plane, as it could be detected on a monitor after a beam deflector. A condition on the energy spread for the visibility of the stripes turns out to be $\sqrt{8\pi}\Delta E < h\nu$. The effect of the laser diffraction is evident for $\Delta t_L \gg R_L/c$ and consists in stopping the emission process and the formation of the stripes.

A qualitative criterion for recognizing the stripe regime is to individuate electron spectra characterized by a strong

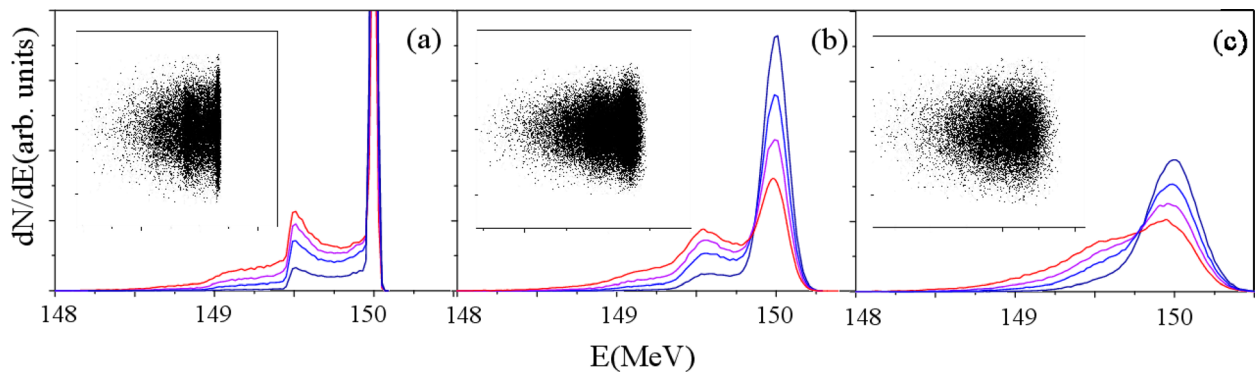


FIG. 4. Electron distribution in arbitrary units as function of the energy E in MeV for different laser time duration, as given by CAIN. Dark blue curve: $\Delta t_L = 0.8$ ps with $E_L = 0.25$ J, light blue curve: $\Delta t_L = 2.4$ ps with $E_L = 0.75$ J, magenta curve: $\Delta t_L = 4.8$ ps with $E_L = 1.5$ J, and red curve: $\Delta t_L = 16$ ps with $E_L = 5$ J. (a) $\Delta E/E = 10^{-4}$; (b) $\Delta E/E = 5 \times 10^{-4}$; (c) $\Delta E/E = 10^{-3}$. In the inner boxes, the electron distribution projected on the x-y plane, as could be seen on a monitor.

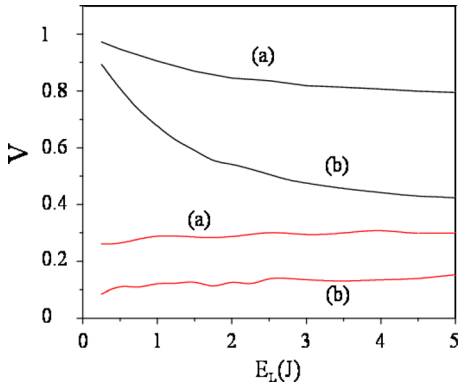


FIG. 5. $V$ as a function of the laser energy $E_L(J)$. (a) $\Delta E/E = 10^{-4}$; (b) $\Delta E/E = 5 \times 10^{-4}$. Black curves: visibility of the peak at $E = 150$ MeV. Red curves: visibility of the peak at $E = 149.5$ MeV.

asymmetry with respect to the core of the beam. A more quantitative parameter for evaluating the visibility of the stripes could be defined as

$$V = \frac{(dN/dE)_{max} - (dN/dE)_{min}}{(dN/dE)_{max} + (dN/dE)_{min}}, \tag{13}$$

where $(dN/dE)_{max}$ is one of the maxima of the curve and $(dN/dE)_{min}$ is a neighboring minimum. Fig. 5 shows the trend of $V$ as function of the laser energy for the peak at 150 MeV, constituting the bulk of the electron beam, and for the secondary peak at 149.5 MeV, corresponding to the electrons that have undergone a first collision. In this last case, values of the visibility of 15%–25% are reached.

## IV. CONCLUSIONS

In conclusion, we think that the point-like nature of the Compton collision between electron and laser photons is revealed by the occurrence of stripes in the electron energy distribution connected to a momentum grouping of the electrons. The master equation derived from the Chapman-Kolmogorov equation for Markov phenomena (7) is suitable to describe this process. A comparison between the results of the master equation and the simulations with the code CAIN validates this theoretical model. An experiment aimed at exploring the electron distribution structure after the scattering is proposed at the PlasmonX source at SPARC-LAB, permitting to have insight into the nature of the collision.

[1]M. Pfeifer, Nature **442**, 63 (2006).
[2]T. Shintake *et al.*, Nat. Photonics **2**, 555 (2008).
[3]Z. Huang *et al.*, Phys. Rev. ST Accel. Beams **13**, 020703 (2010).
[4]L. Giannessi *et al.*, Phys. Rev. ST Accel. Beams **14**, 060712 (2011).
[5]W. Ackermann *et al.*, Nat. Photonics **1**, 336 (2007).
[6]J. Mauritsson *et al.*, Phys. Rev. A **70**, 021801(R) (2004).
[7]M. Bech, O. Bunk, C. David, R. Ruth, J. Rifkin, R. Loewen, I. Feidenhans'l, and F. Pfeier, J. Synchrotron Radiat. **16**, 43 (2009).
[8]M. Babzien *et al.*, Phys. Rev. Lett. **96**, 054802 (2006).
[9]D. J. Gibson, F. Albert, S. G. Anderson, S. M. Betts, M. J. Messerly, H. Phan, V. A. Semenov, M. Shverdin, A. M. Tremaine, F. Hartemann *et al.*, Phys. Rev. ST Accel. Beams **13**, 070703 (2010).
[10]C. Sun and Y. K. Wu, Phys. Rev. ST Accel. Beams **14**, 044701 (2011).
[11]V. Telnov, Phys. Rev. Lett. **78**, 4757 (1997).
[12]E. Esarey, Nucl. Instrum. Methods Phys. Res. A **455**, 7 (2000).
[13]G. Blumenthal and R. Gould, Rev. Mod. Phys. **42**, 237 (1970).
[14]G. R. M. Robb and R. Bonifacio, Europhys. Lett. **94**, 34002 (2011).
[15]A. Kol'chuzhkin, A. Potylitsyn, S. Strokov, and V. Ababiy, Nucl. Instrum. Methods Phys. Res. A **201**, 307 (2003).
[16]E. J. Saldin, E. A. Schneidmiller, and M. V. Yurkov, Nucl. Instrum. Methods Phys. Res. A **381**, 545 (1996).
[17]G. Geloni, V. Kocharyan, and E. Saldin, "On quantum effects in spontaneous emission by a relativistic electron beam in an undulator," DESY Report No. 12-022, 2012, http://arxiv.org/abs/1202.0691.
[18]V. Petrillo *et al.*, Europhys. Lett. **101**, 10008 (2013).
[19]K. Yokoya, KEK Report No. 85–9, 6 Oct 1985.
[20]See http://www-acc-theory.kek.jp/members/cain for CAIN, 1985.
[21]V. Petrillo *et al.*, Nucl. Instrum. Methods Phys. Res. A **693**, 109 (2012).
[22]G. R. M. Robb and R. Bonifacio, Phys. Plasmas **19**, 073101 (2012).
[23]G. Geloni, E. Saldin, and M. V. Yurkov, Europhys. Lett. **98**, 44001 (2012).
[24]A. Potylitsyn and A. Kol'chuzhkin, Europhys. Lett. **100**, 24006 (2012).
[25]J. D. Jackson, *Classical Electrodynamics*, 3rd ed. (Wiley, New York, 1998).
[26]N. G. Van Kampen, *Stochastic processes in Physics and Chemistry* (North Holland Press Library, 1992).
[27]P. Oliva, A. Bacci, U. Bottigli, M. Carpinelli, P. Delogu, M. Ferrario, D. Giulietti, B. Golosio, V. Petrillo, L. Serafini *et al.*, Nucl. Instrum. Methods Phys. Res. A **615**, 93 (2010).
[28]P. Tomassini *et al.*, IEEE Trans. Plasma Sci. **36**, 1782 (2008).
[29]L. Gizzi, A. Bacci, S. Betti *et al.*, Eur. Phys. J. Spec. Top. **175**, 3 (2009).